Published in : ACS Applied Polymer Materials (2025), vol. 7, n°05, pp. 3033–3042
DOI: 10.1021/acsapm.4c03705
Status : Postprint (Author's version)

SOLID POLYMER ELECTROLYTES BASED ON POLY(ETHYLENE OXIDE)/ CARBONATED SOYBEAN OIL BLENDS

Ashish Raj[1], Bruno Grignard[2], Christophe Detrembleur[3], and Jean-François Gohy[4]*

[1]*Institute of Condensed Matter and Nanoscience (IMCN), Université catholique de Louvain, Place L. Pasteur 1, 1348 Louvain-la-Neuve, Belgium*

[2]*Center Center for Education and Research on Macromolecules (CERM), CESAM Research Unit, University of Liège, 4000 Liège, Belgium; Federation of Researcher in Innovation Technologies for CO2 Transformation (FRITCO2T Research Platform), University of Liège, 4000 Liège, Belgium; orcid.org/0000-0002-6016-3317*

[3]*Center for Education and Research on Macromolecules (CERM), CESAM Research Unit, University of Liège, 4000 Liège, Belgium; WEL Research Institute, 1300 Wavre, Belgium; orcid.org/0000-0001-7849-6796*

[4]*Institute of Condensed Matter and Nanoscience (IMCN), Université catholique de Louvain, Place L. Pasteur 1, 1348 Louvain-la-Neuve, Belgium; orcid.org/0000-0003-4169-1883*

*Corresponding author

KEYWORDS: Carbonated soybean oil; LiTFSI; Solid polymer electrolytes; Interface; Lithium batteries

ABSTRACT

Blends of poly(ethylene oxide) and carbonated soybean oil with lithium bis(trifluoromethane sulfonyl)imide salt are investigated here as free-standing solid polymer electrolyte (SPE) membranes. Carbonated soybean oil decreases the crystallinity of poly(ethylene oxide) and confers adhesive nature to the polymer blends, in addition to better interface with electrodes. An ionic conductivity of 3.3 × 10^{-5} S cm^{-1} at room temperature and a broad electrochemical stability window (>4.2 V versus Li/Li^+) are observed for the membranes prepared from those blends, together with a high stability versus lithium metal electrodes as inferred from stripping and plating experiments (for cycling time > 300 h). Subsequently, $LiFePO_4$/polymer blend/lithium metal battery prototypes are assembled and deliver 108 mA h g^{-1} of discharge capacity with high Coulombic efficiency at 0.1C and 60 °C in the first cycle. Here, the trade-offs in poly(ethylene oxide)-based SPEs are addressed with bioderived carbonate-containing molecules contributing toward sustainable materials development.

Published in : ACS Applied Polymer Materials (2025), vol. 7, n°05, pp. 3033–3042
DOI: 10.1021/acsapm.4c03705
Status : Postprint (Author's version)

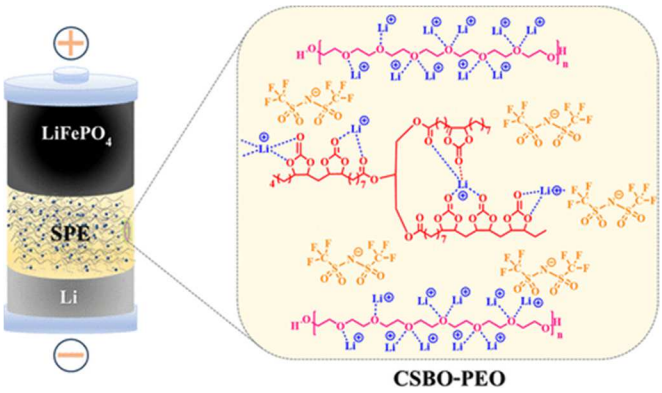

INTRODUCTION

The quest to reach the newer milestone of energy density with adequate cost and safety continues to spark a strong interest in bringing more innovations to the matured and existing Li-ion technology. The original idea of lithium metal as an anode was never dropped in this research area due to its high theoretical capacity (3860 mA h g^{-1}) and lightweight (estimated energy density ∼250 W h kg^{-1}). However, the major obstacle has always been the safety of the battery due to high reactivity, Li dendrite growth, processing, and lack of infrastructure, limiting its commercial use.[1,2] Solid-state batteries (SSBs) based on lithium metal have been eyed upon with huge expectations of overcoming all the underlying hurdles associated with Li metal for superior performance. SSBs are reported to impart lightweight, robustness, flexibility, thermal safety, and recyclability to lithium metal batteries (LMBs) in addition to upheaval in the long life and high performance of the cells.[3,4] Having all of these advantages, the quest for superior solid-state electrolytes has been active for decades even before commercial LIBs came into the market. From 1980 and onward, SSEs such as ceramic-based conductors and organic polymer electrolytes gained momentum. Armand, Wright, and co-workers' efforts led to the discovery of Li^+/Na^+−polymer complexes as potential ion conductors.[5,6] Their revolutionary discovery of poly(ethylene oxide) (PEO)-based solid polymer electrolytes (SPEs) paved the long road of utilizing polymer chemistry for electrolytes. However, designing an SPE with good ionic conductivity, wide electrochemical stability window (ESW), high transference number, decent interface compatibility, and high dielectric constant with superior mechanical and thermal properties remains a challenge until now.[7,8] Addressing this concern, various classes of PEO-based polymers and their alternatives[9,10] have been investigated via smart approaches like grafting,[11−13] block copolymers,[14−16] networks, blends,[17−19] single lithium-ion conducting polymers,[20−22] gel polymers,[23,24] and hybrids.[19,25,26] Potential polymers such as polyesters,[27,28] polycarbonates,[29−31] poly(vinyl alcohol),[32,33] polyurethanes,[34−36] and polysiloxanes,[37,38] just to name a few, have been designed with functionalities involving, e.g., ethers, esters, and carbonates analogous to organic solvents used in liquid electrolytes for over-ruling issues accompanying PEO-based electrolytes.

Cyclic carbonates are quite appropriate for lithium-ion coordination and dissolution due to their superior dielectric constant (≈60−70 for cyclic carbonates vs less than 10 for ethylene oxide at room temperature).[39,40] Coupling cyclic carbonate functionality with ethylene oxide units in copolymers and blends has been investigated as an interesting approach toward SPEs. As a typical example, Tominaga

Published in : ACS Applied Polymer Materials (2025), vol. 7, n°05, pp. 3033–3042
DOI: 10.1021/acsapm.4c03705
Status : Postprint (Author's version)

et al. synthesized a linear poly(ethylene carbonate) that was further integrated into an hybrid membrane reaching an ionic conductivity of ~10^{-5} S cm^{-1} at 30 °C.[31,41] Our research group investigated SPEs based on cyclic carbonate-bearing trifluoro-methacrylate and vinylidene fluoride units[42] and random copolymers of *n*-butyl acrylate and cyclic carbonatebearing acrylate.[43] Xue et al. reported borate-based porous polymer electrolytes containing cyclic carbonates displaying an ionic conductivity of 1.32 × 10^{-3} S cm^{-1} at 30 °C.[44] Mecerreyes and co-workers synthesized a series of poly(ethylene oxide carbonates) by polycondensation between different ethylene oxide diols and dimethyl carbonate that were further investigated as SPEs.[45] An intense amount of work has also been directed toward understanding the interfaces that guide the design of electrolytes. On those trails, interfacial engineering, chain end modification, and coating-stabilized polymers have been explored.[46,47]

Therefore, taking up the challenge to improve the existing PEO-based SPE by combining it with bioderived molecules, we report here blends of PEO and carbonated soybean oil (CSBO), with the synthesis of CSBO reported elsewhere as shown in Scheme 1.[48] Cyclic carbonates with their viscous nature plasticize PEO and are speculated to facilitate blend formation with less crystallinity of PEO and overcome the trade-offs in electrochemical properties. Herein, we compare blended CSBO–PEO and pristine PEO membranes by performing spectroscopic and electrochemical measurements.

Scheme 1. Synthesis of Carbonated Soybean Oil (CSBO) and Its Blending with PEO along with a Simplified Scheme of Molecular Chains Interacting with LiTFSI

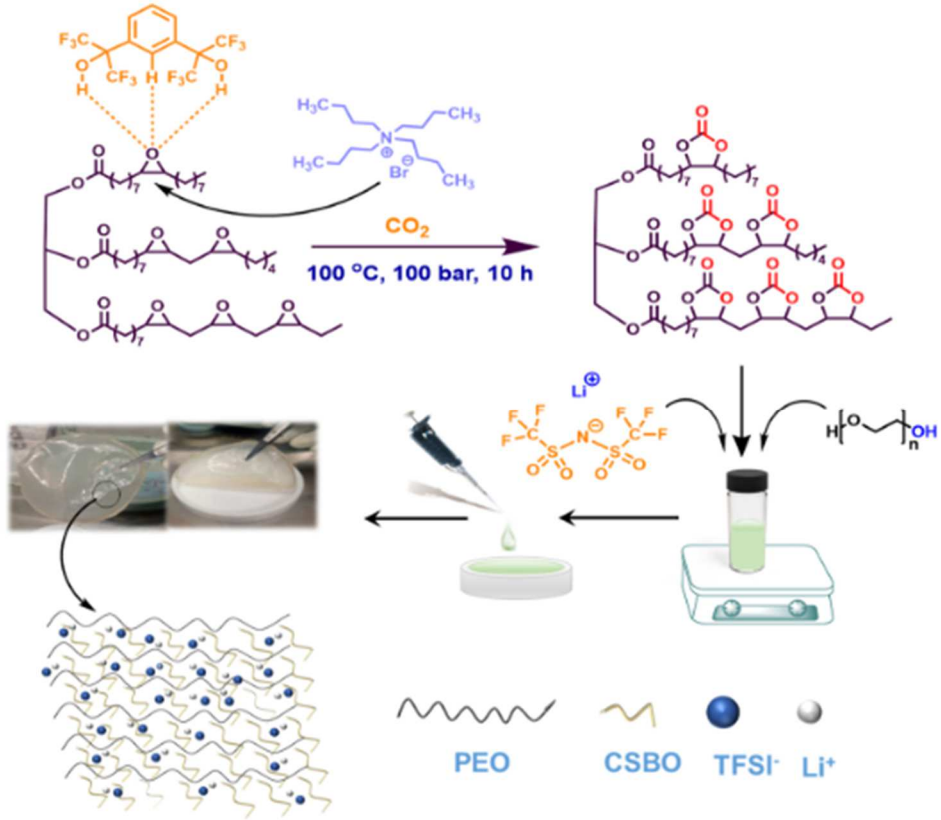

Published in : ACS Applied Polymer Materials (2025), vol. 7, n°05, pp. 3033–3042
DOI: 10.1021/acsapm.4c03705
Status : Postprint (Author's version)

MATERIALS AND METHODS

Materials. Epoxidized soybean oil (ESBO) was obtained from Vandeputte Oleochemicals (Belgium). Carbon dioxide (CO_2, N48) was supplied by Air Liquide. 1,3-Bis(2 hydroxyhexafluoroisopropyl)benzene (HFI) was purchased from Fluorochem. Poly(ethylene oxide) ($M_w \sim 10^6$ g/mol, a crystallinity degree of 81% as measured by differential scanning calorimetry (DSC), and a dispersity of 1.8 as measured by size exclusion chromatography), tetrabutylammonium bromide (TBABr, >99%), propylene carbonate, acetonitrile, bis(trifluoromethane)sulfonimide lithium (LiTFSI), lithium iron phosphate (LFP), and Super P were purchased from Sigma-Aldrich. *N*-Methyl-2-pyrrolidone (NMP) was purchased from Alfa Aesar. A cellulose separator (TF48-50, 50 μm × 66 mm) was supplied by TOB. All reactants and catalysts were used as received, without any further purification. Deuterated chloroform ($CDCl_3$) used for nuclear magnetic resonance (NMR) spectroscopy was purchased from Eurisotop.

Synthesis. *Synthesis of Carbonated Soybean Oil (CSBO).* Biobased carbonated soybean oil (CSBO) was synthesized as reported elsewhere[48] by coupling supercritical CO_2 with epoxidized soybean oil (ESBO) using a bicomponent organocatalytic system that combined TBABr as a catalyst and HFI as an activator. The coupling reaction was performed at 100 °C and 100 bar using 2.5 mol % of organocatalyst (TBAB/HFI = 1 mol/mol) for 10 h. These optimized reaction conditions ensured the fast and full conversion of epoxy into corresponding cyclic carbonates in CBSO (MW ∼ 1250 g/mol).

Synthesis of CSBO−PEO and Electrolyte Films. Samples were denoted by the acronym CSBO−PEO*x* (*y*/*z*), where *y* and *z* are the wt % of CSBO and PEO, respectively, and x is the wt % of added LiTFSI to CBSO-PEO. CSBO−PEO blends were synthesized by mixing various amounts of CSBO and PEO in a vial using acetonitrile solvent, and mixtures were stirred for >6 h, then drop-cast on Teflon molds, and later transferred to a vacuum oven. They were maintained at 70 °C for ≥24 h under dynamic vacuum. The CSBO−PEO SPEs were prepared following a similar procedure, with LiTFSI added to the CSBO−PEO mixtures prior to solvent evaporation. The dried membranes were peeled off from the molds in the glovebox as depicted in **Scheme 1**. All of the structural and thermal characterizations were performed on polymers without a separator. In addition to free-standing membranes, the polymer solutions were also drop-cast on cellulose paper for separator-supported membranes. All membranes were cut in disks with a diameter of 16 mm and with a thickness in the range 50−200 μm.

Materials Characterization. *Nuclear Magnetic Resonance.* NMR spectroscopy was conducted by using a Bruker 300 UltraShield spectrometer. The monomers and polymers were dissolved in deuterated chloroform.

Fourier Transform Infrared Spectra (FTIR) Measurements. FTIR measurements were carried out on a PerkinElmer spectrometer equipped with a diamond attenuated transmission reflectance device, 8 scans were recorded for each sample over the range of 4000−500 cm^{-1} with a normal resolution of 4 cm^{-1}, and spectra were analyzed with the Spectra Quanta software.

Rheology. Rheological properties of samples were measured on an ARES (Advanced Rheometric Expansion System) Rheometric Scientific rheometer.

Differential Scanning Calorimetry. DSC was conducted using a Mettler Toledo DSC1 instrument equipped with STARe software. Samples were placed in a 40 μL sealed aluminum pan. The temperature profile was swept from −70 to 100 °C at a heating rate of 10 °C min^{-1} under a nitrogen atmosphere.

Thermogravimetric Analysis (TGA). TGA was conducted using a Mettler Toledo TGA. Samples were placed in an 85 μL alumina crucible under a constant argon flow with a heating rate of 5 K min^{-1}, and the initial and final temperatures were set at 25 and 600 °C, respectively.

X-ray Photoelectron Spectroscopy. X-ray photoelectron spectroscopy (XPS) was performed using an SSI X-Probe (SSX 100/206) photoelectron spectrometer from Surface Science Instruments equipped with a monochromated Al Kα (200 W) X-ray source. The batteries were disassembled, and samples

Published in : ACS Applied Polymer Materials (2025), vol. 7, n°05, pp. 3033–3042
DOI: 10.1021/acsapm.4c03705
Status : Postprint (Author's version)

were mounted on an XPS sample holder in a glovebox prior to being transferred to the XPS vacuum chamber in the flux of an argon atmosphere. All binding energies were calculated relative to the C−H component of the C 1s peak fixed at 284.8 eV. Data analysis was carried out using the CasaXPS software. For the survey scan, a 1.0 eV step size and a 0.1 eV step size were used for high-resolution scans for all elements with 150 energy steps.

Electrochemical Measurements. Electrochemical analysis by potentiostatic electrochemical impedance spectroscopy (PEIS), linear sweep voltammetry (LSV), chronoamperometry, and galvanostatic cycling potential limitation were carried out on Biologic BCS-COM and VMP3 multichannel potentiostats using CR2032 coin or Swagelok cells. All electrochemical measurements were repeated at least five times on three specimens of the same sample to ensure the reproducibility of the results.

Potentiostatic Electrochemical Impedance Spectroscopy. The ionic conductivity of investigated SPEs was determined by PEIS for symmetric stainless steel (SS|SPE|SS) with the PTFE ring in Swagelok cells in the frequency range of 7−50 MHz, with an applied single sinusoidal A.C. excitation voltage of 10 mV. The temperature dependence measurements were carried out from 20 to 100 °C by gradually increasing the temperature at the rate of 0.33 °C min^{-1}. One h was waited between each measurement to reach an equilibrium state.

Linear Sweep Voltammetry. Measurements were performed at various temperatures on asymmetric CR2032 coin cells as (Li|SPE|Al) and (Li|SPE|SS|) over the potential range of 0−6 V (vs Li/Li^+) at the scan rate of 1 mV s^{-1} at 30 °C.

Transference Number (t_{Li^+}). Transference number measurements were carried out on symmetric lithium metal cells (Li|SPE|Li) fabricated over various membranes following the Bruce−Vincent method. Chronoamperometry with a D.C. voltage of 10 mV was performed followed by PEIS measurements in the frequency range of 7−50 MHz, at 10 mV of A.C. excitation voltage at 30 °C. PEIS measurements were recorded before and after steady state (before and after polarization).

Stripping and Plating. The symmetric cell Li|SPE|Li was fabricated for stripping and plating analysis. The cells were charged and discharged for 1 h each for multiple cycles with a current density of 1 μA cm^{-2} and cutoff voltages +4 V and −4 V at room temperature.

Galvanostatic Cycling Potential Limitation. Galvanostatic charge−discharge cycling and rate capability measurements for the Li|SPE|LFP cells were tested. The slurry for the cathodes was prepared from LFP, Super P, PEO, PEO/CBSO-PEO, and NMP via grinding using a mortar pestle and cast on Al-foil/carbon with the doctor-blade technique. The coated slurry was dried in an air oven for more than 6 h at 60 °C prior to vacuum drying at 120 °C for more than 24 h. The cathode compositions were maintained to the weight ratios of 6:2:1:1 and 7:2:1 for LFP, Super P, and PEO, respectively. The cathode and anode were cut into a diameter of 14 mm for electrolyte films with a diameter of 16 mm for the cell assembly.

RESULTS AND DISCUSSION

The CSBO−PEO blends investigated in this study were prepared, as shown in **Scheme 1**. The synthesis and structure of the CBSO molecule have been reported elsewhere[48] and are depicted in **Scheme 1**. Each CSBO unit possesses on average six cyclic carbonates, but not all of them are equally accessible to lithium-ion coordination owing to the structure and steric hindrance highlighting the need of additional lithium-conducting functionality, which will be provided by the ether groups of PEO. The other role of adding PEO is to reinforce the mechanical properties of the CSBO-LiTFSI electrolytes since

Published in : ACS Applied Polymer Materials (2025), vol. 7, n°05, pp. 3033–3042
DOI: 10.1021/acsapm.4c03705
Status : Postprint (Author's version)

those ones behave as viscous liquids.[49] On the other hand, CSBO can be considered as a plasticizing additive for PEO-LiTFSI SPEs and could also decrease the crystallinity of PEO. Thus, a synergistic effect on the ionic conductivity is expected by blending CSBO and PEO in the same SPE.

Electrolytes prepared from CSBO with LiTFSI demonstrated amorphous and adhesive nature and promising ionic conductivity at RT as reported in our previous work.[49] There were further blended here with PEO. However, the viscous nature of CSBO did not allow less than 40% of PEO in the blend for self-standing membranes to be obtained. The accordingly obtained blends were observed to be softer and more flexible as compared to pristine PEO with and without LiTFSI. This is confirmed by comparing rheological measurements on the pristine PEO SPE membrane to the CSBO−PEO 50:50 wt/wt blended membrane, both of them being loaded with 20 wt % LiTFSI (**Figure S1**). The obtained results demonstrate that the addition of CSBO results, as expected, in weaker mechanical properties for the plasticized SPE membrane since the storage modulus G' is significantly higher for the PEO membrane compared to the CSBO−PEO one. However, both membranes show G' higher than the loss moduli G'' in the whole investigated frequency range and G' values in the 10^5–10^6 Pa range which are acceptable for further use in SSBs (**Figure S1**). To control the thickness and avoid short circuit at higher temperature above the melting point of the investigated electrolyte, cellulose support was added during membrane preparation. Furthermore, free-standing polymer blends and cellulose-supported membranes were assured solvent-free by sufficient drying in the vacuum oven at >24 h at 70 °C. Blends with percentages of PEO varying from 100% to 50% by weight were prepared with CSBO.

FTIR measurements of the CSBO−PEO blends were recorded, as shown in **Figure S2**. The carbonate of CC rings was not opened, as confirmed from the stretching band at 1796 cm^{-1} for pure CBSO which shifts to 1801 cm^{-1} for CSBO− PEO (10:90). Another carbonyl corresponding to the ester groups of CSBO was detected at 1739 cm^{-1} with a slight shift at 1741 cm^{-1} for all of the blends. The broadening of the bands at 1280 and 1240 cm^{-1} for CSBO−PEO (40:60 and 50:50, respectively) can be explained by a lower number of available C−O ether units for Li^+ complexation than that for other samples (**Figure S2a**). The characteristic bands for LiTFSI were observed at 1188 cm^{-1} from SO_2 asymmetric stretching.[50,51] Further focusing on the IR spectra of CSBO−PEO (50:50) with added salt, broadening in the signals was observed with an increase in salt concentration, which also resulted in increased softness of the blend. As shown in the highlighted region of **Figure S1b** corresponding to the CO band around 1800 cm^{-1}, a shift toward lower frequency could be witnessed as salt concentration increases due to Li^+ ion interaction with carbonyl, while dissociation of LiTFSI was assured superior in all samples ranging from 10 wt % to 30 wt %.

The investigated CSBO−PEO blends and related SPEs have been measured by DSC to determine their glass-transition temperature (T_g), melting temperature (T_m), and crystallization temperature (T_c). Typical DSC curves are shown in **Figure S3**. Of particular importance is the T_g, the lower it is, the higher is the chain segmental motion in the polymer and the better will be the mobility of ions in the SPE.[52] Almost all the samples demonstrated a T_g around −34 °C except CSBO−PEO (50:50 wt/wt) with a T_g at −48 °C. Those results confirm the plasticizing effect of CSBO toward PEO and the miscibility between CSBO and PEO. It is worth mentioning that a rather high content of CSBO is required to trigger the plasticizing effect. The miscibility between PEO and CSBO is further illustrated by the effect of the addition of increasing CSBO amount on the crystalline behavior of PEO. First, T_m continued to decrease from 63 to 46 °C for 100 wt % PEO to 50 wt % PEO loading in the blend (**Figure S3a**). Second, the

Published in : ACS Applied Polymer Materials (2025), vol. 7, n°05, pp. 3033–3042
DOI: 10.1021/acsapm.4c03705
Status : Postprint (Author's version)

crystallization degree of PEO decreased as the CSBO amount in the blend increased and almost vanished for the CSBO−PEO (50:50 wt/wt) blend (**Figure S3a**). Both observations again confirm the miscibility of CSBO with PEO and the anticipated beneficial effect on the ionic conductivity of the CSBO−PEO blends due to increased PEO segment mobility and decreased PEO crystallinity, especially for the CSBO−PEO (50:50 wt/wt) sample. Further measurements were performed for the CSBO−PEO (50:50 wt/wt) blend as a function of LiTFSI concentration. Both T_m and T_g first decreased with an increasing salt concentration (**Figure S3b**). The T_g decreased from −11 to −46 °C from 10 to 20 wt % of added salt, indicating that relatively low amounts of added salt have a plasticizing effect on the polymer matrix. For 30 wt % of added LiTFSI, the crystalline behavior of PEO disappears but T_g increases to −37 °C, a temperature well below RT. This behavior is fully in line with previously reported results.[15,16]

The thermal degradation of the CBSO-PEO (50:50 wt/wt) blend was investigated by TGA with and without LiTFSI, as shown in **Figure S3c**. The initial increment beyond 100% weight can be attributed to the decomposition of adsorbed water. The decomposition of PEO starts at 185 °C, while for PEO-LiTFSI, it starts at 199 °C in one and two stages, respectively. The degradation temperature was increased with added LiTFSI for PEO and vice versa for the CSBO−PEO blend. However, the decomposition (T_d) for CSBO−PEO starts at 293 °C and decreased to 238 °C with addition of salt in a reverse trend with two and three stages, respectively. The decomposition of LiTFSI salt could be observed beyond 400 °C for both blend and pure PEO. Nevertheless, it is assured that the reported electrolyte could be utilized safely for cell operation beyond 238 °C without decomposition.

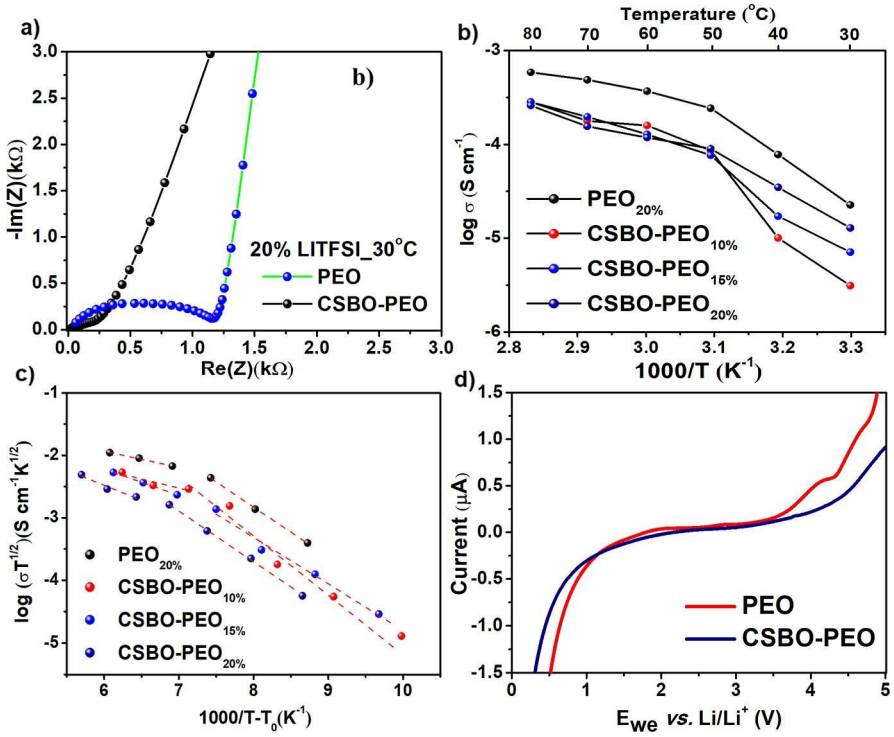

Figure 1. (a) Nyquist plots of PEO and CSBO−PEO (50:50 wt/wt) symmetric cells at 30 °C; (b) temperature-dependent ionic conductivity of CSBO−PEO (50:50 wt/wt, subscript indicates wt % LiTFSI) in comparison to $PEO_{20\%}$; (c) temperature-dependent ionic conductivity using the VFT model; and (d) LSV comparison of PEO and CSBO−PEO composite with 20% LiTFSI at 60 °C.

Published in : ACS Applied Polymer Materials (2025), vol. 7, n°05, pp. 3033–3042
DOI: 10.1021/acsapm.4c03705
Status : Postprint (Author's version)

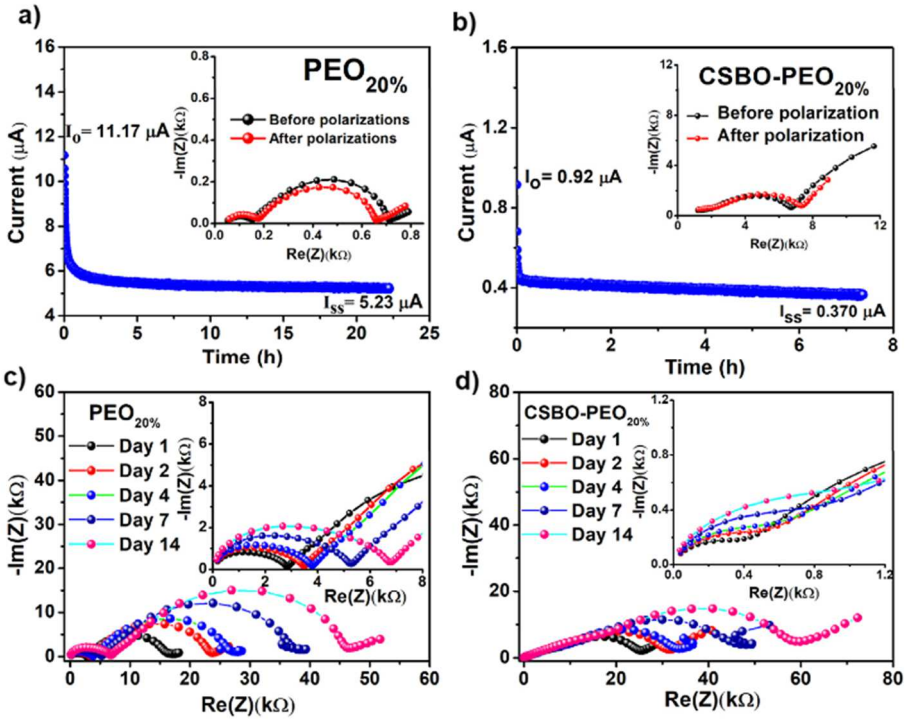

Figure 2. (a,b) Transference number measurement using chronoamperometry (D.C. polarization), followed by AC PEIS in the inset and (c,d) aging studies: PEIS with time at open-circuit potential (OCP) both the Li|$PEO_{20\%}$|Li cell and Li|CSBO–$PEO_{20\%}$|Li cells, respectively (CSBO–PEO 50:50 wt/wt, subscript indicating wt % of LiTFSI, magnified plot in the inset).

The ionic conductivities of the investigated SPEs were obtained from Nyquist plots by performing potential electrical impedance spectroscopy (PEIS) at various temperatures with 10 to 20 wt % of added LiTFSI as shown in **Figure 1a** for the CSBO–PEO (50:50 wt/wt) sample. It was found that when the concentration of PEO in the blend increases, conductivity also increases as depicted in **Figure S4a**. **Equation 1** has been used for the calculation of the ionic conductivities (σ)

$$\sigma = \frac{l}{RS} \qquad (1)$$

where R is the bulk electrolyte Ohmic resistance from AC impedance and l and S are the thickness and the surface area of the analyzed SPE membrane, respectively. The CSBO–$PEO_{20\%}$ membrane showed a conductivity of 1.3×10^{-5} S cm^{-1} yet lesser than the pure PEO electrolyte with 2.3×10^{-5} S cm^{-1} at room temperature. In all the CSBO–PEO blend samples, the conductivity was increased with temperature until 80 °C (**Figure 1b**), and the error in conductivity values was measured to be less than 5%. The conductivity follows another linear regime from 60 °C onward, which could be explained by the melting of the PEO crystalline domains as highlighted in DSC curves. At elevated temperature, CSBO–PEO samples with lower salt concentration outperform CSBO–PEO20% slightly. This could be explained by the higher ion pairing and ion concentration gradient in a higher salt concentration electrolyte.

Published in : ACS Applied Polymer Materials (2025), vol. 7, n°05, pp. 3033–3042
DOI: 10.1021/acsapm.4c03705
Status : Postprint (Author's version)

Nevertheless, the 20 wt % LiTFSI amount was chosen for both blend and pure PEO with a conductivity of 1.2×10^{-4} and 3.7×10^{-4} S cm^{-1}, respectively, at 60 °C, for charge and discharge experiments owing to balance between the mechanical properties and charge carriers. In this respect, SPE membranes with 20 wt % LiTFSI were quite flexible and easy to handle, while SPEs with higher salt loading were leading to brittle membranes.

Moreover, the conductivity of SPEs did not seem to align well with Arrhenius behavior following a linear regime upon the inverse of temperature. Therefore, the following data have also been fitted by using the Vogel−Fulcher−Tamman (VFT) equation (**eq 2**) within the 30−80 °C temperature range.

$$\sigma T^{1/2} = A e^{-\frac{E}{k_b(T - T_0)}} \quad (2)$$

where A is the pre-exponential factor, T is the absolute temperature, T_0 is the Vogel scaling temperature at which the free volume disappears or at which free entropy becomes zero, T_0 is related to T_g by T_g-50 K following an approximation, E_α is the pseudoactivation energy of ion transport, and k_b is the Boltzmann constant.[53,54] This model could be often informative on unravelling the effect of segmental motion on the overall conductivity above T_g.[55] Like Arrhenius plots, VFT plots also show nonlinear behavior, which has been fit into two components, i.e., 20 − 60 °C (region 1) and 60 − 80 °C (region 2). The activation energy calculated from the slope of the VFT plot and **eq 2** is observed to decrease with salt concentration for CSBO−PEO SPEs as obtained from **Figure 1c**. The lowest E_{a1} of −14.3 kJ/mol for CSBO−$PEO_{15\%}$ was calculated to be higher than that for $PEO_{20\%}$-SPE at −15.4 kJ/ mol within the same temperature range. However, clear increasing trend in E_{a2} was witnessed at higher temperature above melting, in the order of $PEO_{20\%}$ (−4.9 kJ/mol) < CSBO−$PEO_{10\%}$ (−5.6 kJ/mol) < CSBO−$PEO_{15\%}$ (−8.0 kJ/ mol) < CSBO−$PEO_{20\%}$ (−9.2 kJ/mol) favoring chain and ion mobility with less hindrance. The structure of CSBO indicates that all cyclic carbonate rings are not equidistant from each other and could block the Li^+ ions due to both carbonyl and ether oxygen coordination. That could support that the inclusion of CSBO in the PEO matrix lowered the mobility of Li ions, preventing their fast release for hopping. Nevertheless, those results clearly indicate that the addition of PEO is boosting the ionic conductivity of CSBO, which is far higher in the CSBO−PEO SPEs compared to the pristine $CSBO_{20\%}$based SPE reported earlier,[49] despite the shift in the physical state of the electrolyte from oily CSBO to solid CSBO−PEO films. **Table S1** in the Supporting Information shows the E_{a1} and E_{a2} calculated for the SPEs along with the pre-exponential factor and R^2 as the corresponding fitting coefficient. These conductivity measurements were carried out with free-standing SPE films, while a comparative plot as indicated in **Figure S4b** highlights that conductivity was decreased when PEO and blends were prepared with a cellulose separator.

The ESW of SPEs was investigated by performing LSV. The pure $PEO_{20\%}$ and CSBO−$PEO_{20\%}$ SPEs were submitted to a constant scan rate of 1 mV/s in the range of 0−5 V versus Li/ Li^+ at 60 °C as shown in **Figure 1d**. A lithium metal chip and aluminum foil were chosen as the negative and positive electrodes, respectively. The CSBO−$PEO_{20\%}$ sample showed an oxidative potential >4.2 V compared to <4 V for the SPE based on pure PEO. There was no noticeable redox peak observed for both SPEs in the lower voltage range. The following analysis confirmed that inclusion of CSBO led to the decrease in the oxidation of PEO with lithium metal boosting the lithium electrolyte interface compatibility. Partial

Published in : ACS Applied Polymer Materials (2025), vol. 7, n°05, pp. 3033–3042
DOI: 10.1021/acsapm.4c03705
Status : Postprint (Author's version)

degradation of CSBO in contact with lithium metal is believed to play a key role in the formation of a stable SEI and could also prevent or decrease further degradation of PEO. Moreover with a slight compromise in the conductivity, we could be able to achieve higher ESW and hence offer interesting electrolyte candidates for higher voltage positive electrodes.

A high t_{Li^+} is advantageous for long-term cycling batteries, allowing efficient Li^+ ion transport and lower Coulombic efficiency loss. The transference number (t_{Li^+}) of lithium cations in nonblocking Li|SPE|Li cells was determined here by AC impedance combined with DC polarization. The t_{Li^+} value was calculated using the Bruce−Vincent method,[56,57] following **eq 3**

$$t_{Li^+} = \frac{I_{ss}(V - I_0R_0)}{I_0(V - I_{ss}R_{ss})} \quad (3)$$

where V is the D.C.-applied potential and I_0 and I_{ss} are the initial and steady-state currents recorded with R_0 and R_{ss} as initial and steady-state interfacial resistances from PEIS measurements at an A.C. sinusoidal voltage of 10 mV. The chronoamperometry plots are shown in **Figure 2a,b** with impedance before and after polarization for both SPEs at 60 °C. The current values cannot be numerically compared due to different thicknesses of both SPEs. As a result of constant potential of 10 mV, the interfacial resistance decreased from 713 to 659 Ω, while current varies from an initial value of 11.2 μA to a stabilized value of 5.2 μA, which led to the calculation of the t_{Li^+} value to be 0.15 ± 0.04 for PEO films. The t_{Li^+} of the CSBO−PEO (50:50 wt/wt) SPE was calculated to be 0.36 ± 0.04 at 60 °C from **Figure 2b** with interfacial resistance increasing from 2026 to 2087 Ω and initial current from 0.9 to 0.4 μA of steady-state current.

The PEIS measurement as a function of time is recorded to track the effect of reactive species at the electrode surface. This is often performed at OCP to analyze the effect of aging at the bulk and interface level. For SSBs, another interesting investigation revolves around the absence or minimal formation of lithium dendrites. We performed aging analysis via Nyquist plots as shown in **Figure 2c**,d at RT and OCP after equilibrating both cells at 60 °C.

The resistance was dropped in the case of CSBO−PEO after prolonged heating due to the change in the thickness of the electrolyte membrane, while this phenomenon was less pronounced in the case of the PEO membrane. The percentage increases in electrolytic resistance and interfacial resistance from day 1 to day 14 were 139% and 172% for PEO, respectively. However, it was recorded to be 152% and 137% in the case of CSBO−PEO (refer to **Table S2** for resistance values). The less pronounced semicircle in the latter case could be attributed to an imperfect geometrical capacitive behavior within the bulk of the electrolyte of the soft CSBO−PEO membrane. The increase in the electrolyte resistance can be related to the higher reactivity of carbonates in the blend membrane. However, the lower percentage increase in interfacial resistance compared with the PEO membrane can be attributed to the formation of an optimized SEI at the lithium metal surface in the presence of CSBO.

The stability of our SPEs has also been qualitatively studied via long-term stripping and plating of lithium for a symmetric Li|SPE|Li cell. Galvanostatic charge−discharge for 1 h each was performed for each cell held at 60 °C in a climate chamber followed by 6 h of rest at the current densities of 6.25, 12.5, 25, and 50 μA cm^{-2} for more than 45 cycles each, respectively. Both SPE-based cells recorded similar overpotentials of ∼25 and ∼23 mV for PEO and CSBO−PEO, respectively, which increased

Published in : ACS Applied Polymer Materials (2025), vol. 7, n°05, pp. 3033–3042
DOI: 10.1021/acsapm.4c03705
Status : Postprint (Author's version)

consistently to ~45 and ~47 mV at 12.5 μA cm^{-2}. Upon further increment in the current density to 50 μA cm^{-2}, a trivial elevation of overpotential to ~190 mV was observed as shown in **Figure 3**. The constant overpotential recorded over more than 300 cycles hints at the formation of a stable SEI. With these findings, it could be speculated that the investigated SPEs could facilitate high Coulombic efficiency and reversibility of lithium-ion transport across the electrolyte. However, with the stripping and plating experiment of lithium with both SPEs at mentioned current densities, it is still not clear to discriminate the effect of CSBO into the CBSO−PEO blend.

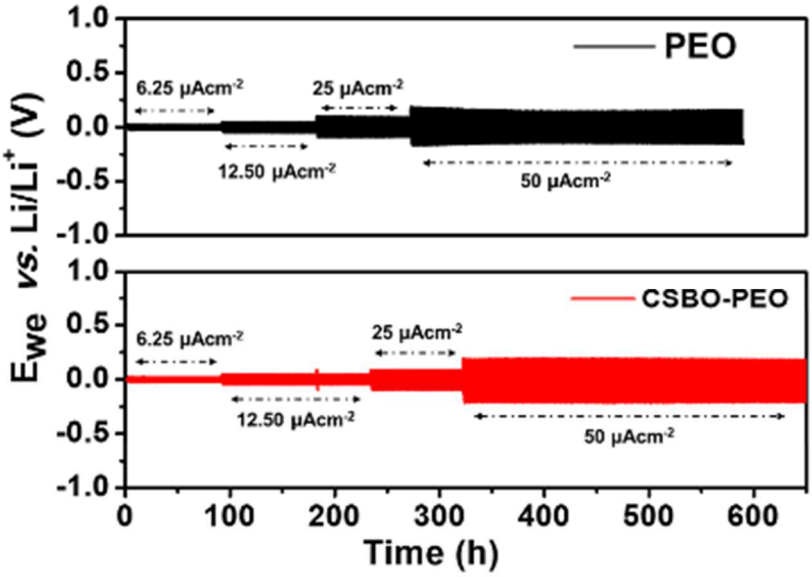

Figure 3. Galvanostatic charge−discharge voltage profiles for stripping−plating at various current densities at 60 °C with Li|SPE| Li symmetric cells. SPEs are PEO (top) and CSBO/PEO 50:50 wt/wt (bottom), both SPEs loaded with 20 wt % LiTFSI.

The investigated SPEs have been further tested in LMB prototypes with LFP cathodes. The PEO and CSBO−PEO membranes were combined with cellulose separators for controlled thickness (coined as SPE@CP). Galvanostatic charge−discharge curves of those lithium metal batteries between cutoff voltages of 4 to 2 V at 60 °C via constant current cycling are depicted in **Figure 4**. With the CSBO−PEO SPEs, specific discharge capacities of 108, 105, and 99 mA h g^{-1} were achieved for the first, 100th, and 250th cycles at 0.1C, respectively (**Figure 4a**). In contrast, SPEs based on PEO at 0.1C delivered 90, 103, and 74 mA h g^{-1} corresponding to the first, 50th, and 100th discharge cycles, and they further continued to decay as shown in **Figure 4b**. Although the performances of CSBO−PEO SPEs were superior to pure PEO SPEs, higher polarizations were observed in former than latter. Polarizations of < ~0.3 V and ~0.1 V were recorded during the first cycle, while they decreased to ~0.28 V and ~0.06 V in subsequent 100th cycles for CSBO−PEO and PEO SPEs, respectively. The lower polarization in the case of PEO SPEs can be supported by their slightly higher conductivity, and the decrement of the overpotentials could be credited to the stabilization of the SEI at the lithium metal. The capacity fading was clearly observed in the case of PEO SPEs after 25 cycles onward with a calculated capacity retention of <80% after 125 cycles, whereas 93% were recorded for CSBO−PEO SPEs after 200 cycles (**Figure 4c**).

Published in : ACS Applied Polymer Materials (2025), vol. 7, n°05, pp. 3033–3042
DOI: 10.1021/acsapm.4c03705
Status : Postprint (Author's version)

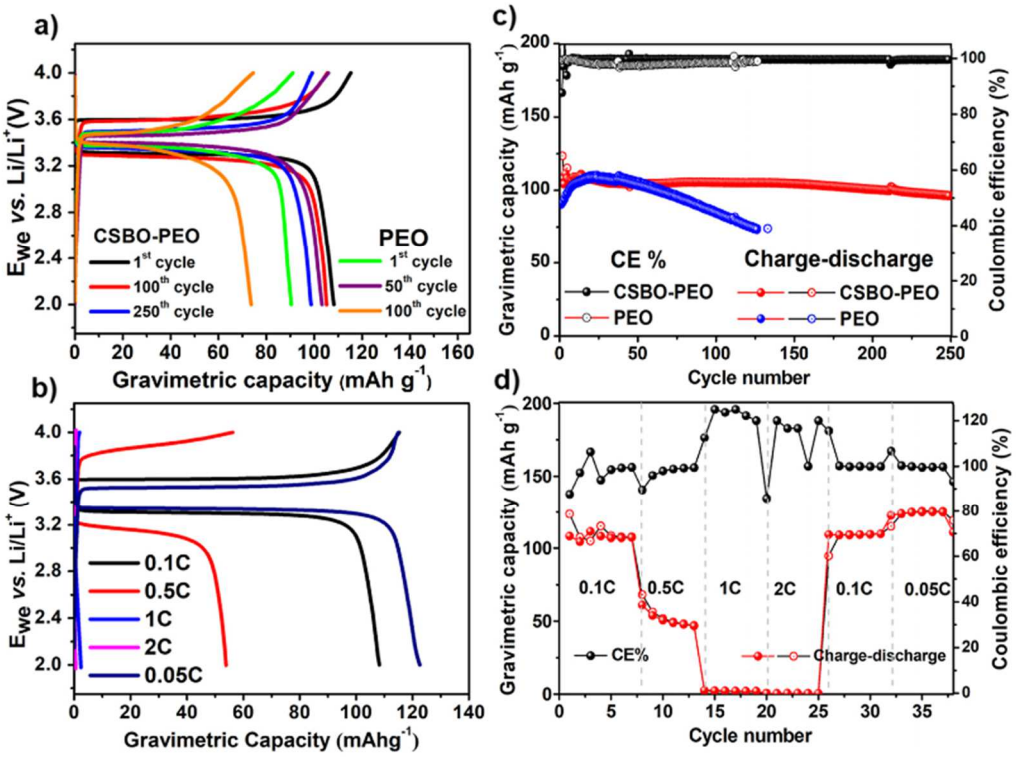

Figure 4. (a) Galvanostatic charge−discharge voltage profiles for Li|SPE@CP|LFP cells based on PEO (20 wt % LiTFSI) and CSBO−PEO (50:50 wt/wt and 20 wt % LiTFSI) SPEs at 0.05C, 60 °C during the following cycles; (b) capacity retention plot with cycle number 0.05C at 60 °C; (c) galvanostatic charge−discharge voltage profiles at different C-rates; and (d) rate capability plot with different C-rates for Li|CSBO-PEO@CP|LFP.

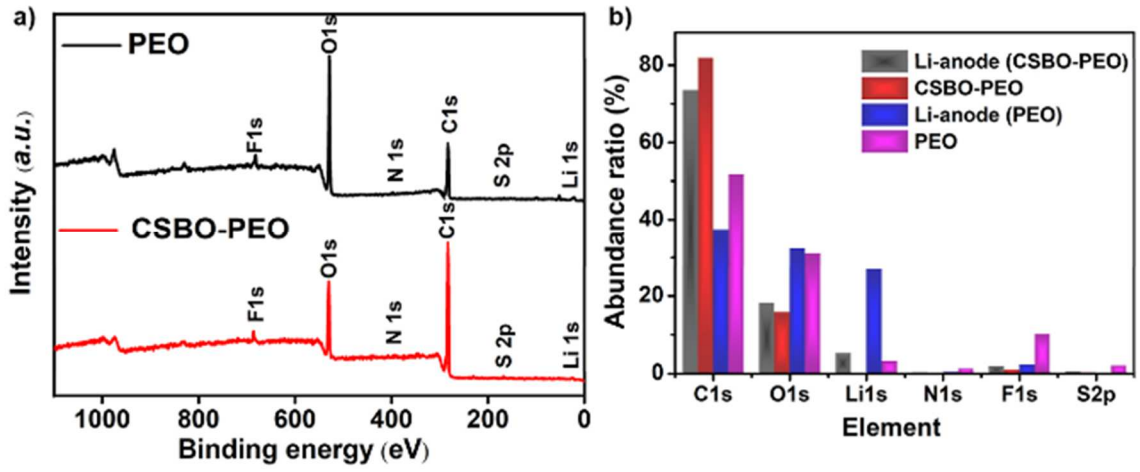

Figure 5. (a) Survey spectrum of the Li anode of PEO and the CSBO−PEO SPE-based Li-LFP cells after 100+ cycling and (b) abundance ratio percentage of surface elements constituting SEI for the Li anode and corresponding SPE membranes.

Coulombic efficiency was more than 98% during most of the cycles, which supports the efficient mobility of lithium ions (**Figure 4c,d**). We also tested cells with our SPEs without cellulose support at a lower temperature of 40 °C in a climate chamber at 0.1C which witnessed a slightly higher polarization of 0.37 V during the initial cycle (**Figure S5**).

Published in : ACS Applied Polymer Materials (2025), vol. 7, n°05, pp. 3033–3042
DOI: 10.1021/acsapm.4c03705
Status : Postprint (Author's version)

Finally, a qualitative yet comparative post-mortem investigation has been attempted on cycled cells based on either PEO or PEO−CSBO blend in a Li|SPE@CP|LFP cell configuration. Both SPE-based cells were cycled for >100 cycles at 0.1C at 60 °C prior to post-mortem analysis. HR-XPS measurements were performed on the surface of cycled Li− metal and SPEs from PEO and CSBO−PEO-based cells. The abundance percentage highlighted the majority of carbon and oxygen elements in both SPEs and survey spectra (**Figure 5a,b**).

However, a lower percentage of carbon is detected for the PEO cell relatively with higher lithium content, meaning the SEI of the PEO cell contains less carbon species including adventitious carbon due to lower reactivity than the CSBO− PEO blend. On the other hand, a higher amount of fluorine is detected for the PEO than for the blend one, indicating more decomposition of LiTFSI. The HR-XPS spectra for comparative Li−metal surfaces have been depicted in **Figure 6**.

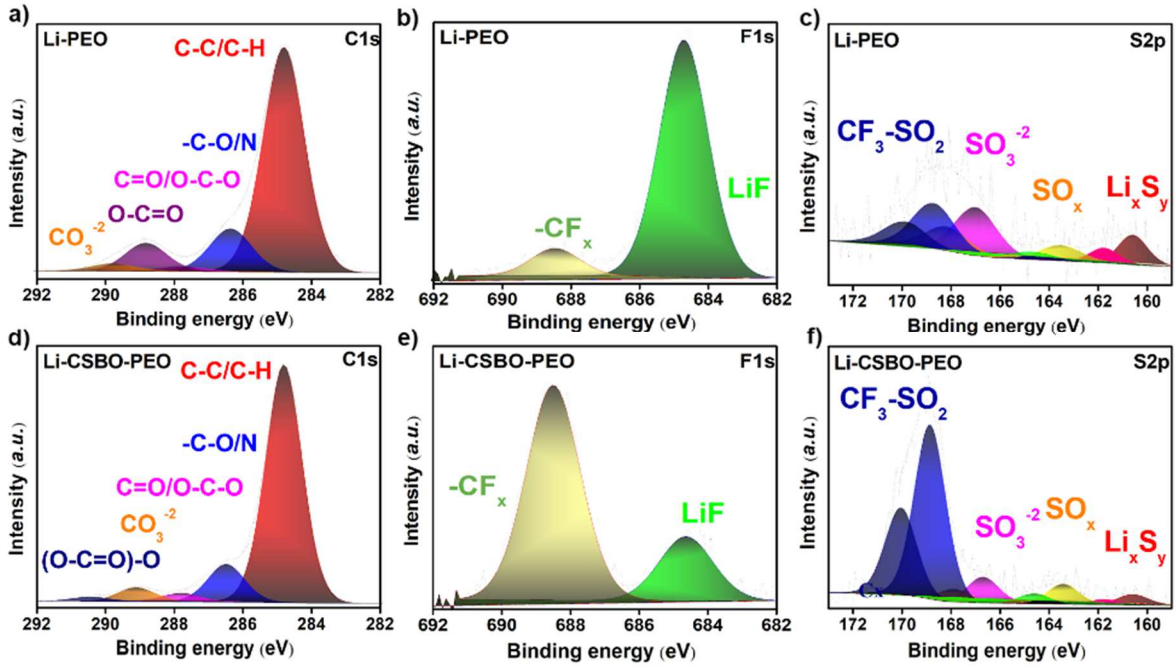

Figure 6. HR-XPS of (a,d) carbon, (b,e) fluorine, and (c,f) sulfur for the lithium anode surface of PEO and CSBO−PEO cells after cycling with LFP, respectively.

HR-XPS of C 1s indicates peaks at 284.8, 286.4, 287.7, 288.7, and 289.7 eV for C−C/C−H, C−O/N, O−C−O/C=O, O−C=O, and CO_3^{2-}, respectively, in the PEO cell and at 284.8, 286.4, 287.8, 289.1, and 290.4 eV corresponding to C−C/C−H, C−O/N, O−C−O/C=O, CO_3^{-2}, and −(O−C=O)−O−, respectively, for the CSBO−PEO cell (**Figure 6a,d**).[46] Those results confirm that organic carbonates in CSBO have a higher reactivity toward lithium metal than PEO and largely contributes to the formation of stable SEI in the case of the CSBO−PEO cell. As far as the F 1s spectra are concerned, the PEO cell recorded higher decomposition of LiTFSI to LiF (1.9% at 684.7 eV and 0.2% of CF_3 at 688.5 eV, **Figure 6e**) compared to the CSBO−PEO cell (0.5% of LiF at 684.6 and 1.5% of CF_3 at 688.5 eV, **Figure 6b**).[58] Higher CF_3 content in the CSBO−PEO cell might be credited to lower LiTFSI decomposition (as well as catalyst involved in the synthesis of CSBO) due to $TFSI^-$ ions trapped around the CC rings resulting in a lower concentration gradient at the surface as highlighted above. The sulfur, S 2p from the SEI of both SPEs is deconvoluted

Published in : ACS Applied Polymer Materials (2025), vol. 7, n°05, pp. 3033–3042
DOI: 10.1021/acsapm.4c03705
Status : Postprint (Author's version)

into four species in double splitting involving CF_3–SO_2, SO_4^{-2}, SO_x, and sulfides in the B.E. of ∼168.7 eV−160.6 eV, respectively (**Figure 6c,f**) evolving from LiTFSI.[59]

Other elemental HR-XPS of N 1s, O 1s, and Li 1s are provided in the Supporting Information, **Figure S6**, along with quantification **Table S3**. Again, a higher fluoride content was detected in the case of the PEO cell with more $-CF_3$ than LiF due to limited reactivity of LiTFSI and higher concentration gradients as a contrary to the CSBO−PEO blend cell. To summarize, we discovered that addition of CSBO to PEO decreases the reactivity of PEO chains, which benefits the superior Li transport, broadened ESW, along with a stable SEI layer at the anode.

CONCLUSIONS

We have reported here the SPE membranes obtained from CSBO and PEO via a blending approach. CBSO−PEO blends offered lower brittleness, slight adhesiveness, and thus good interfacial contact with electrodes compared to PEO-based SPEs. The addition of CSBO was found to substantially decrease the crystallinity of PEO in the accordingly obtained SPE membranes. Coin cells were fabricated using either self-standing or thickness-controlled cellulose-supported SPE membranes for electrochemical measurements. The inclusion of CSBO molecules did not result in the increase in the conductivity of blended membranes but rather offered crucial properties like extension of ESW to >4.2 V for blends in relative <3.9 V for PEO versus Li/Li^+. The presence of carbonated moieties is believed to contribute to the beneficial decomposition of the electrolytes at the electrodes for SEI and to lower subsequent undesired reactions with lithium metal. In our investigation, we found that the transference number was increased to more than double for the CSBO−PEO blend, which is supposed to significantly improve the charge− discharge performance of the further investigated LFP-based cells. Indeed, CSBO−PEO-containing cells delivered stable cycling of LFP cathodes with lithium metal beyond 250 cycles with a high capacity in contrast to capacity fading in the case of PEO-LFP cells. In the post-mortem analysis, the lithium metal reactivity and the resulting decomposed electrolytic species were confirmed as well as the crucial role of CSBO decomposition in forming a stable SEI. The attempts to increase the green footprint and sustainability of the electrolyte were successfully achieved in this work and would encourage more efforts in the future to match the required expectations of SSBs with high energy and power density.

Published in : ACS Applied Polymer Materials (2025), vol. 7, n°05, pp. 3033–3042
DOI: 10.1021/acsapm.4c03705
Status : Postprint (Author's version)

***Figure S1**. Rheology of PEO and CSBO-PEO (50:50 wt:wt) SPE membranes loaded with 20 wt% LiTFSI for storage (G') and loss (G'') modulus, Tan δ versus angular frequency.*

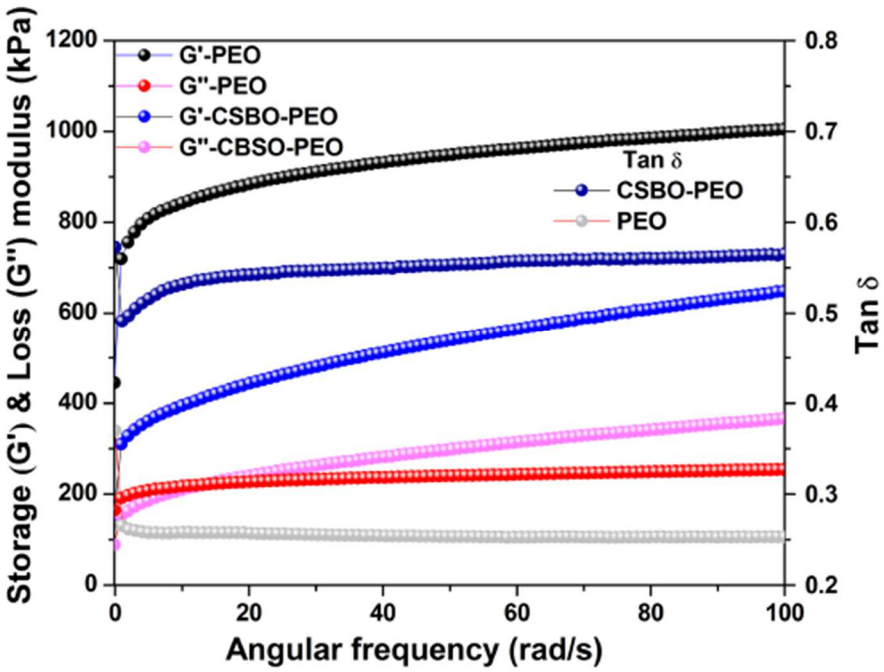

***Figure S2.** a) Comparative FTIR spectra of CSBO, PEO and CSBO-PEO (wt:wt) blends with various formulations, respectively with 20 wt% of LiTFSI; and b) FTIR of CSBO-PEO (50:50 wt:wt) blends with various amounts LiTFSI (in subscript in wt%).*

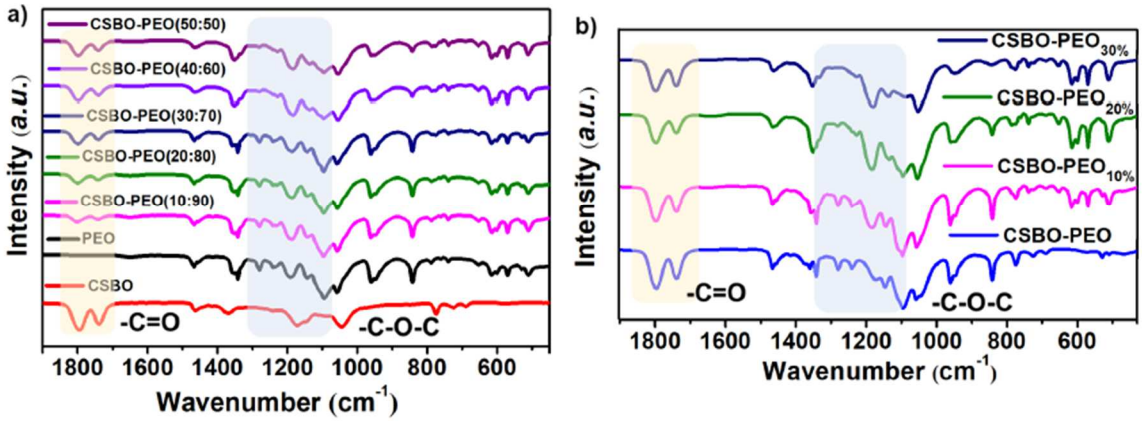

Published in : ACS Applied Polymer Materials (2025), vol. 7, n°05, pp. 3033–3042
DOI: 10.1021/acsapm.4c03705
Status : Postprint (Author's version)

Figure S3. *DSC thermograms of SPE membranes, a) different compositions of CSBO-PEO (y:z wt:wt) with LITFSI (20 wt%); b) CSBO-PEO (50:50 wt:wt) with LiTFSI (wt% in subscript); and c) Thermogravimetric analysis of PEO and CSBO-PEO (50:50 wt:wt) with and without LiTFSI, respectively.*

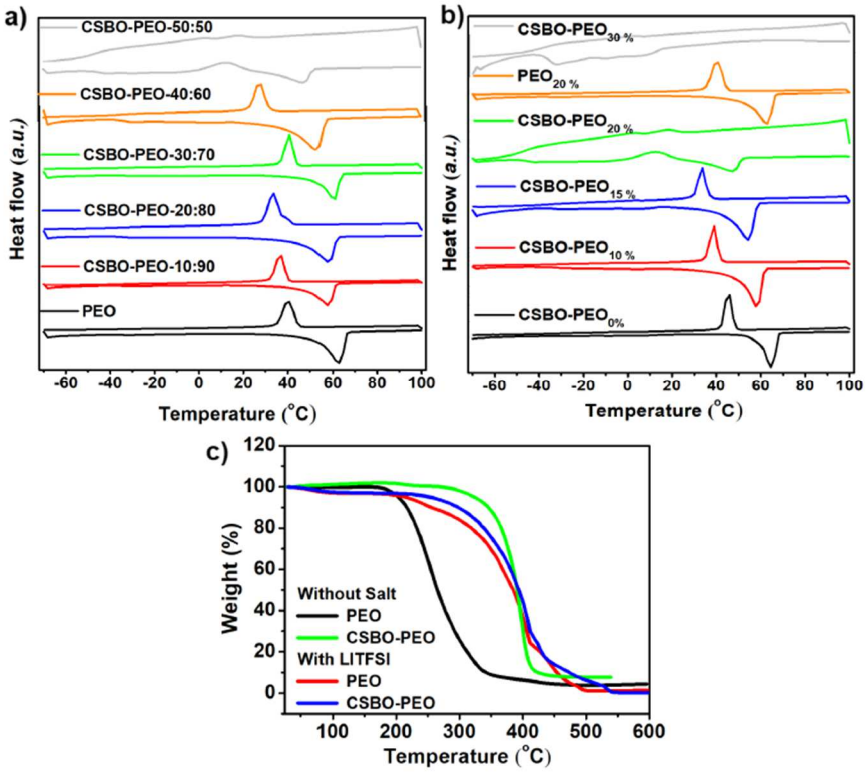

Figure S4. *Temperature dependent ionic conductivity of SPEs with 20% of LiTFSI, a) y:z: by wt% in comparison to PEO, and b) with and without cellulose separator (CP: cellulose paper, without CP: film), respectively.*

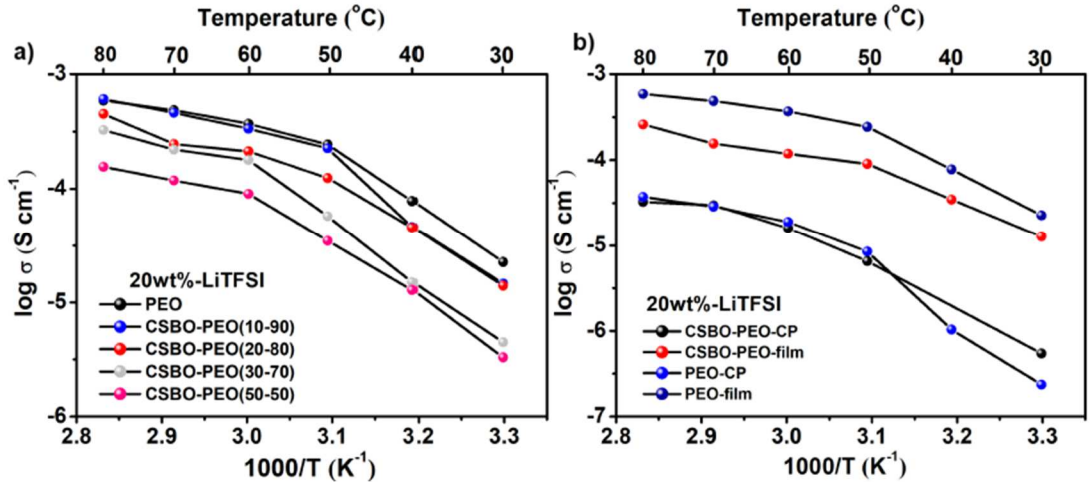

Published in : ACS Applied Polymer Materials (2025), vol. 7, n°05, pp. 3033–3042
DOI: 10.1021/acsapm.4c03705
Status : Postprint (Author's version)

Figure S5. *a) Galvanostatic charge-discharge voltage profile with gravimetric capacity at following charge and discharge of 1st, 50th and 100th at 0.1C and b) Capacity retention plot with cycle number for Li|CSBO-PEO$_{20\%}$|LFP at 40 °C.*

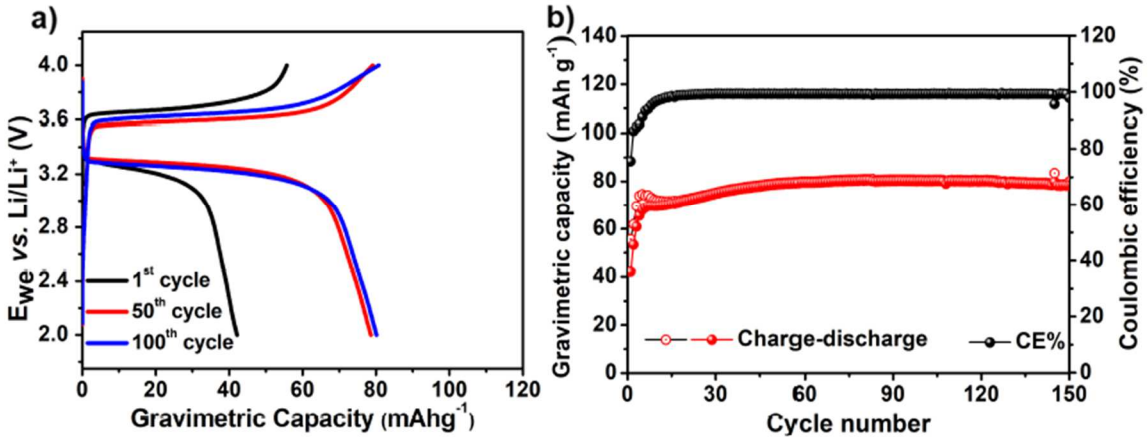

Figure S6. *HR-XPS of a) and d) Oxygen (O1s), b) and e) Nitrogen (N1s), c) and f) Lithium (Li1s), for Li-anode surface of cell based on PEO and CSBO-PEO, respectively.*

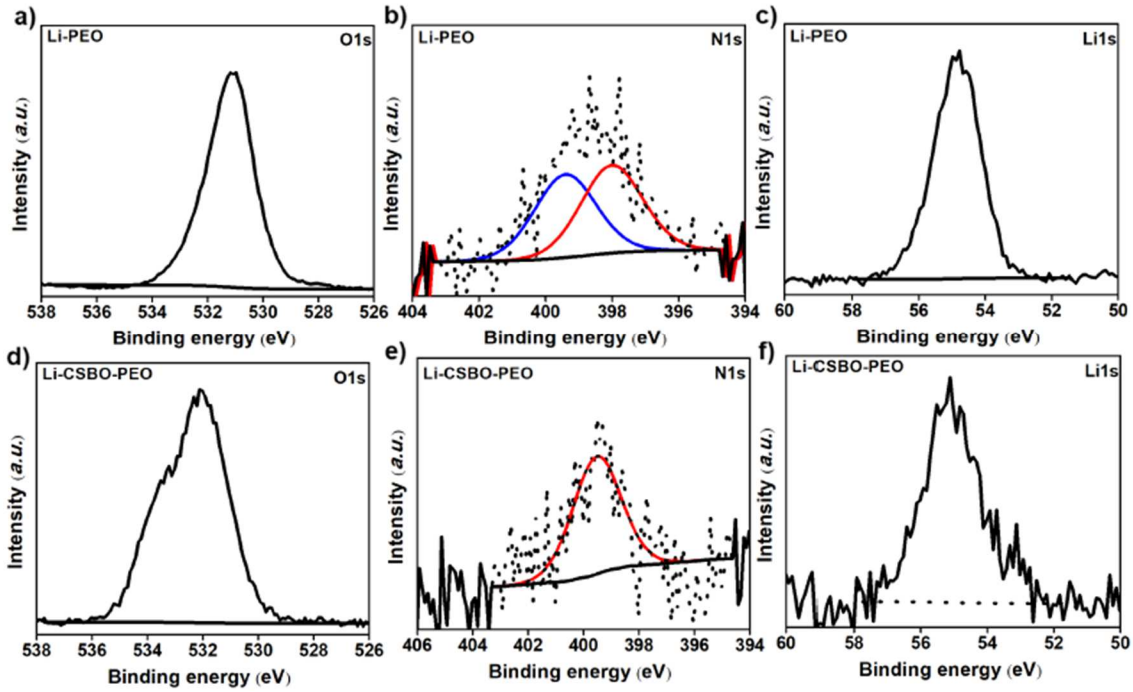

Published in : ACS Applied Polymer Materials (2025), vol. 7, n°05, pp. 3033–3042
DOI: 10.1021/acsapm.4c03705
Status : Postprint (Author's version)

Table S1. *Activation energy and pre-exponential factor as calculated from the two-region linear fitting of VFT plots (region 1 and region 2 correspond to lower (20 °C - 50 °C) and higher temperature (60 °C - 80 °C), respectively).*

CSBO-PEO (1:1)	Adj. R_1^2	Adj. R_2^2	lnA_1	lnA_1	E_{a1} (kJ-mol^{-1})	E_{a2} (kJ-mol^{-1})
PEO	0.99	0.99	5.0	-0.4	-15.4	-4.9
10%	0.91	0.75	4.3	-0.5	-19.8	-5.6
15%	0.98	0.99	2.6	0.3	-14.3	-8.0
20%	0.99	0.92	2.8	0.4	-15.5	-9.2

Table S2. *Aging analysis: Interfacial (R_{in}) and bulk (R_b) résistance. (in Ohm) of the symmetric Li-Li cells at OCP.*

Day	at OCP			
	$PEO_{20\%}$		$CSBO\text{-}PEO_{20\%}$	
	R_b	R_{in}	R_b	R_{in}
1st	2836	17185	362	25267
2nd	3489	23687	432	31579
4th	3799	27934	531	33645
7th	5283	38323	858	48160
14th	6769	46708	912	59864

Table S3. *Quantification table of XPS analysis of Li-anode post-cycling indicating binding energy (BE), fUll width half maxima (FWHM) and abundance ratio (%).*

		F 1s			O 1s	N 1s			C 1s						S $2p_{3/2}$	Li 1s
		F-C	F-Li	F total		NH^+-(C,H)	N-(C,H)	N total	O-C=O/CO_3^{-2}	O-C=O/CO_3^-	O=C/--O-C-O-	C-(O,N)	C-(C,H)	C total		
Li-PEO-cycled	BE	688.46	684.71		530.98	399.4	398.01		289.79	288.82	287.8	286.36	284.8			54.78
	FWHM	1.676	1.676		1.898	2.174	2.174		1.43	1.43	1.43	1.43	1.43			1.609
	A%	0.233	1.999	**2.232**	**32.241**	0.185	0.195	**0.38**	0.891	3.395	0.577	5.164	27.315	**37.342**	**0.199**	**26.991**
Li-CSBO-PEO-cycled	BE	688.5	684.63		532.12	399.53			290.44	289.1	287.8	286.48	284.8			55.12
	FWHM	1.85	1.85		2.911	2.055			1.257	1.257	1.257	1.257	1.257			1.624
	A%	1.511	0.451	**1.962**	**18.228**	0.301		**0.301**	1.049	3.375	2.023	9.103	57.971	**73.521**	**0.469**	**5.246**

Published in : ACS Applied Polymer Materials (2025), vol. 7, n°05, pp. 3033–3042
DOI: 10.1021/acsapm.4c03705
Status : Postprint (Author's version)

ASSOCIATED CONTENT

* SUPPORTING INFORMATION

The Supporting Information is available free of charge at https://pubs.acs.org/doi/10.1021/acsapm.4c03705.

Rheological measurements of SPEs; FTIR spectra of SPEs; DSC thermograms and TGA of SPE membranes; temperature-dependent ionic conductivity measurements; galvanostatic charge−discharge curves; HR-XPS spectra; activation energies calculated from VTF plots; interfacial resistance as a function of aging; and quantification table of XPS analysis (PDF)

AUTHOR CONTRIBUTIONS

The manuscript was written through contributions of all authors. All authors have given approval to the final version of the manuscript.

Notes

The authors declare no competing financial interest.

ACKNOWLEDGMENTS

A.R. and JFG are grateful to INNOVIRIS for supporting this research in the frame of a BRIDGE project. C.D. is FRS-FNRS Research Director. The authors thank Maxime Bourguignon (CERM, University of Liege) for performing rheological measurements.

REFERENCES

(1) Su, L.; Manthiram, A. Lithium-Metal Batteries via Suppressing Li Dendrite Growth and Improving Coulombic Efficiency. *Small Structures* 2022, *3* (10), 2200114.
(2) Aslam, M. K.; Niu, Y.; Hussain, T.; Tabassum, H.; Tang, W.; Xu, M.; Ahuja, R. How to avoid dendrite formation in metal batteries: Innovative strategies for dendrite suppression. *Nano Energy* 2021, *86*, 106142.
(3) Takada, K. Progress and prospective of solid-state lithium batteries. *Acta Mater.* 2013, *61* (3), 759−770.
(4) Varzi, A.; Raccichini, R.; Passerini, S.; Scrosati, B. Challenges and prospects of the role of solid electrolytes in the revitalization of lithium metal batteries. *J. Mater. Chem. A* 2016, *4* (44), 17251− 17259.
(5) Armand, M. The history of polymer electrolytes. *Solid State Ionics* 1994, *69* (3), 309−319.
(6) Payne, D. R.; Wright, P. V. Morphology and ionic conductivity of some lithium ion complexes with poly(ethylene oxide). *Polymer* 1982, *23* (5), 690−693.
(7) Grundish, N. S.; Goodenough, J. B.; Khani, H. Designing composite polymer electrolytes for all-solid-state lithium batteries. *Curr. Opin. Electrochem.* 2021, *30*, 100828.
(8) Agrawal, R. C.; Pandey, G. P. Solid polymer electrolytes: materials designing and all-solid-state battery applications: an overview. *J. Phys. D: Appl. Phys.* 2008, *41* (22), 223001.
(9) Xue, Z.; He, D.; Xie, X. Poly(ethylene oxide)-based electrolytes for lithium-ion batteries. *J. Mater. Chem. A* 2015, *3* (38), 19218− 19253.
(10) Yue, L.; Ma, J.; Zhang, J.; Zhao, J.; Dong, S.; Liu, Z.; Cui, G.; Chen, L. All solid-state polymer electrolytes for high-performance lithium ion batteries. *Energy Storage Materials* 2016, *5*, 139−164.

Published in : ACS Applied Polymer Materials (2025), vol. 7, n°05, pp. 3033–3042
DOI: 10.1021/acsapm.4c03705
Status : Postprint (Author's version)

(11) Wright, P. V. Polymer electrolytesthe early days. *Electrochim. Acta* 1998, *43* (10), 1137−1143.
(12) Murata, K.; Izuchi, S.; Yoshihisa, Y. An overview of the research and development of solid polymer electrolyte batteries. *Electrochim. Acta* 2000, *45* (8), 1501−1508.
(13) Meng, N.; Lian, F.; Cui, G. Macromolecular Design of Lithium Conductive Polymer as Electrolyte for Solid-State Lithium Batteries. *Small* 2021, *17* (3), 2005762.
(14) Ghosh, A.; Wang, C.; Kofinas, P. Block Copolymer Solid Battery Electrolyte with High Li-Ion Transference Number. *J. Electrochem. Soc.* 2010, *157*, A846−A849.
(15) Young, W.-S.; Kuan, W.-F.; Epps, T. H. Block copolymer electrolytes for rechargeable lithium batteries. *J. Polym. Sci., Part B: Polym. Phys.* 2014, *52* (1), 1−16.
(16) Rolland, J.; Brassinne, J.; Bourgeois, J. P.; Poggi, E.; Vlad, A.; Gohy, J. F. Chemically anchored liquid-PEO based block copolymer electrolytes for solid-state lithium-ion batteries. *J. Mater. Chem. A* 2014, *2* (30), 11839−11846.
(17) Manuel Stephan, A.; Nahm, K. S. Review on composite polymer electrolytes for lithium batteries. *Polymer* 2006, *47* (16), 5952−5964.
(18) Ngai, K. S.; Ramesh, S.; Ramesh, K.; Juan, J. C. A review of polymer electrolytes: fundamental, approaches and applications. *Ionics* 2016, *22* (8), 1259−1279.
(19) Tang, S.; Guo, W.; Fu, Y. Advances in Composite Polymer Electrolytes for Lithium Batteries and Beyond. *Adv. Energy Mater.* 2021, *11* (2), 2000802.
(20) Gao, J.; Wang, C.; Han, D.-W.; Shin, D.-M. Single-ion conducting polymer electrolytes as a key jigsaw piece for nextgeneration battery applications. *Chem. Sci.* 2021, *12* (40), 13248− 13272.
(21) Zhu, J.; Zhang, Z.; Zhao, S.; Westover, A. S.; Belharouak, I.; Cao, P.-F. Single-Ion Conducting Polymer Electrolytes for Solid-State Lithium−Metal Batteries: Design, Performance, and Challenges. *Adv. Energy Mater.* 2021, *11* (14), 2003836.
(22) Zhang, H.; Li, C.; Piszcz, M.; Coya, E.; Rojo, T.; RodriguezMartinez, L. M.; Armand, M.; Zhou, Z. Single lithium-ion conducting solid polymer electrolytes: advances and perspectives. *Chem. Soc. Rev.* 2017, *46* (3), 797−815.
(23) Manuel Stephan, A. Review on gel polymer electrolytes for lithium batteries. *Eur. Polym. J.* 2006, *42* (1), 21−42.
(24) Zhu, M.; Wu, J.; Wang, Y.; Song, M.; Long, L.; Siyal, S. H.; Yang, X.; Sui, G. Recent advances in gel polymer electrolyte for highperformance lithium batteries. *J. Energy Chem.* 2019, *37*, 126−142.
(25) Liang, J.; Luo, J.; Sun, Q.; Yang, X.; Li, R.; Sun, X. Recent progress on solid-state hybrid electrolytes for solid-state lithium batteries. *Energy Storage Materials* 2019, *21*, 308−334.
(26) Fan, P.; Liu, H.; Marosz, V.; Samuels, N. T.; Suib, S. L.; Sun, L.; Liao, L. High Performance Composite Polymer Electrolytes for Lithium-Ion Batteries. *Adv. Funct. Mater.* 2021, *31* (23), 2101380.
(27) Mindemark, J.; Törmä, E.; Sun, B.; Brandell, D. Copolymers of trimethylene carbonate and *ε*-caprolactone as electrolytes for lithiumion batteries. *Polymer* 2015, *63*, 91−98.
(28) Lin, C.-K.; Wu, I. D. Investigating the effect of interaction behavior on the ionic conductivity of Polyester/LiClO4 blend systems. *Polymer* 2011, *52* (18), 4106−4113.
(29) Mindemark, J.; Lacey, M. J.; Bowden, T.; Brandell, D. Beyond PEOAlternative host materials for Li+-conducting solid polymer electrolytes. *Prog. Polym. Sci.* 2018, *81*, 114−143.
(30) Zhang, J.; Yang, J.; Dong, T.; Zhang, M.; Chai, J.; Dong, S.; Wu, T.; Zhou, X.; Cui, G. Aliphatic Polycarbonate-Based Solid-State Polymer Electrolytes for Advanced Lithium Batteries: Advances and Perspective. *Small* 2018, *14* (36), 1800821.
(31) Kimura, K.; Yajima, M.; Tominaga, Y. A highly-concentrated poly(ethylene carbonate)-based electrolyte for all-solid-state Li battery working at room temperature. *Electrochem. Commun.* 2016, *66*, 46−48.
(32) Every, H. A.; Zhou, F.; Forsyth, M.; MacFarlane, D. R. Lithium ion mobility in poly(vinyl alcohol) based polymer electrolytes as determined by 7Li NMR spectroscopy. *Electrochim. Acta* 1998, *43* (10), 1465−1469.
(33) Zhu, Y. S.; Wang, X. J.; Hou, Y. Y.; Gao, X. W.; Liu, L. L.; Wu, Y. P.; Shimizu, M. A new single-ion polymer electrolyte based on polyvinyl alcohol for lithium ion batteries. *Electrochim. Acta* 2013, *87*, 113−118.
(34) Lv, Z.; Tang, Y.; Dong, S.; Zhou, Q.; Cui, G. Polyurethanebased polymer electrolytes for lithium Batteries: Advances and perspectives. *Chem. Eng. J.* 2022, *430*, 132659.
(35) Misenan, M. S. M.; Khiar, A. S. A.; Eren, T. Polyurethane-based polymer electrolyte for lithium ion batteries: a review. *Polym. Int.* 2022, *71* (7), 751−769.
(36) Raj, A.; Grignard, B.; Detrembleur, C.; Gohy, J.-F. Polyhydroxy Urethanes and Carbonates Bearing Bio-Based Solid Electrolyte for Solid-State Lithium Batteries. *ECS Meeting Abstracts* 2022, *MA202202* (4), 493.
(37) Lin, Y.; Li, J.; Lai, Y.; Yuan, C.; Cheng, Y.; Liu, J. A wider temperature range polymer electrolyte for all-solid-state lithium ion batteries. *RSC Adv.* 2013, *3* (27), 10722−10730.
(38) Wang, Q.; Zhang, H.; Cui, Z.; Zhou, Q.; Shangguan, X.; Tian, S.; Zhou, X.; Cui, G. Siloxane-based polymer electrolytes for solidstate lithium batteries. *Energy Storage Materials* 2019, *23*, 466−490.
(39) Payne, R.; Theodorou, I. E. Dielectric properties and relaxation in ethylene carbonate and propylene carbonate. *J. Phys. Chem.* 1972, *76* (20), 2892−2900.
(40) Chernyak, Y. Dielectric Constant, Dipole Moment, and Solubility Parameters of Some Cyclic Acid Esters. *J. Chem. Eng. Data* 2006, *51* (2), 416−418.

Published in : ACS Applied Polymer Materials (2025), vol. 7, n°05, pp. 3033–3042
DOI: 10.1021/acsapm.4c03705
Status : Postprint (Author's version)

(41) Tominaga, Y.; Nanthana, V.; Tohyama, D. Ionic conduction in poly(ethylene carbonate)-based rubbery electrolytes including lithium salts. *Polym. J.* 2012, *44* (12), 1155−1158.
(42) Boujioui, F.; Zhuge, F.; Damerow, H.; Wehbi, M.; Améduri, B.; Gohy, J.-F. Solid polymer electrolytes from a fluorinated copolymer bearing cyclic carbonate pendant groups. *J. Mater. Chem. A* 2018, *6* (18), 8514−8522.
(43) Boujioui, F.; Damerow, H.; Zhuge, F.; Gohy, J.-F. Solid Polymer Electrolytes Based on Copolymers of Cyclic Carbonate Acrylate and n-Butylacrylate. *Macromol. Chem. Phys.* 2020, *221* (6), 1900556.
(44) Zhou, B.; Zhou, Y.; Lai, L.; Chen, Z.; Li, J.; Jiang, Y.; Liu, J.; Wang, Z.; Xue, Z. Fabrication of Borate-Based Porous Polymer Electrolytes Containing Cyclic Carbonate for High-Performance Lithium Metal Batteries. *ACS Appl. Energy Mater.* 2021, *4* (9), 9582−9593.
(45) Meabe, L.; Huynh, T. V.; Lago, N.; Sardon, H.; Li, C.; O'Dell, L. A.; Armand, M.; Forsyth, M.; Mecerreyes, D. Poly(ethylene oxide carbonates) Solid Polymer Electrolytes for Lithium Batteries. *Electrochim. Acta* 2018, *264*, 367−375.
(46) Bekaert, L.; Raj, A.; Gohy, J.-F.; Hubin, A.; De Proft, F.; Mamme, M. H. Assessing the Long-Term Reactivity to Achieve Compatible Electrolyte−Electrode Interfaces for Solid-State Rechargeable Lithium Batteries Using First-Principles Calculations. *J. Phys. Chem. C* 2022, *126* (19), 8227−8237.
(47) Raj, A.; Panchireddy, S.; Bekaert, L.; Grignard, B.; Detrembleur, C.; Gohy, J.-F. Solid Polymer Electrolytes with Sacrificial End Groups for a Wide Oxidative Potential and Stable Interface in Lithium Metal Batteries. *ACS Appl. Mater. Interfaces* 2024, *16* (36), 47464−47476.
(48) Panchireddy, S.; Grignard, B.; Thomassin, J.-M.; Jérôme, C.; Detrembleur, C. Bio-based poly(hydroxyurethane) glues for metal substrates. *Polym. Chem.* 2018, *9*, 2650.
(49) Raj, A.; Panchireddy, S.; Grignard, B.; Detrembleur, C.; Gohy, J.-F. Bio-Based Solid Electrolytes Bearing Cyclic Carbonates for SolidState Lithium Metal Batteries. *ChemSusChem* 2022, *15* (18), No. e202200913.
(50) Rey, I.; Lassegues, J. C.; Grondin, J.; Servant, L. Infrared and Raman study of the PEO-LiTFSI polymer electrolyte. *Electrochim. Acta* 1998, *43* (10), 1505−1510.
(51) Wong, D. H. C.; Vitale, A.; Devaux, D.; Taylor, A.; Pandya, A. A.; Hallinan, D. T.; Thelen, J. L.; Mecham, S. J.; Lux, S. F.; Lapides, A. M.; Resnick, P. R.; Meyer, T. J.; Kostecki, R. M.; Balsara, N. P.; DeSimone, J. M. Phase Behavior and Electrochemical Characterization of Blends of Perfluoropolyether, Poly(ethylene glycol), and a Lithium Salt. *Chem. Mater.* 2015, *27* (2), 597−603.
(52) Golodnitsky, D.; Strauss, E.; Peled, E.; Greenbaum, S. ReviewOn Order and Disorder in Polymer Electrolytes. *J. Electrochem. Soc.* 2015, *162* (14), A2551.
(53) *Polymer Electrolyte Reviews*, MacCallum, J. R.; Vincent, C. A., Eds.;Elsevier: Londen, 1987.
(54) Karan, N. K.; Pradhan, D. K.; Thomas, R.; Natesan, B.; Katiyar, R. S. Solid polymer electrolytes based on polyethylene oxide and lithium trifluoro- methane sulfonate (PEO−LiCF3SO3): Ionic conductivity and dielectric relaxation. *Solid State Ionics* 2008, *179* (19), 689−696.
(55) Miyamoto, T.; Shibayama, K. Free-volume model for ionic conductivity in polymers. *J. Appl. Phys.* 1973, *44* (12), 5372−5376.
(56) Evans, J.; Vincent, C. A.; Bruce, P. G. Electrochemical measurement of transference numbers in polymer electrolytes. *Polymer* 1987, *28* (13), 2324−2328.
(57) Bruce, P. G.; Vincent, C. A. Steady state current flow in solid binary electrolyte cells. *J. Electroanal. Chem. Interfacial Electrochem.* 1987, *225* (1), 1−17.
(58) Grissa, R.; Fernandez, V.; Fairley, N.; Hamon, J.; Stephant, N.; Rolland, J.; Bouchet, R.; Lecuyer, M.; Deschamps, M.; Guyomard, D.; Moreau, P. XPS and SEM-EDX Study of Electrolyte Nature Effect on Li Electrode in Lithium Metal Batteries. *ACS Appl. Energy Mater.* 2018, *1* (10), 5694−5702.
(59) Chu, H.; Noh, H.; Kim, Y.-J.; Yuk, S.; Lee, J.-H.; Lee, J.; Kwack, H.; Kim, Y.; Yang, D.-K.; Kim, H.-T. Achieving three-dimensional lithium sulfide growth in lithium-sulfur batteries using high-donornumber anions. *Nat. Commun.* 2019, *10* (1), 188.